Biogeosciences, 10, 5255–5266, 2013
www.biogeosciences.net/10/5255/2013/
doi:10.5194/bg-10-5255-2013
© Author(s) 2013. CC Attribution 3.0 License.

Biogeosciences Open Access

Cyanobacterial calcification in modern microbialites at the submicrometer scale

E. Couradeau[1,2,3,*], K. Benzerara[1], E. Gérard[3], I. Estève[1], D. Moreira[2], R. Tavera[4], and P. López-García[2]

[1]Institut de Mineralogie et de Physique des Milieux Condenses UMR7590, Paris, France
[2]Laboratoire Ecologie Systematique Evolution UMR8079, Orsay, France
[3]Institut de Physique du Globe de Paris UMR7154, Paris, France
[4]Departamento de Ecología y Recursos Naturales, Universidad Nacional Autónoma de México, DF Mexico, Mexico
[*]now at: Arizona State University, Tempe, Arizona, USA

Correspondence to: E. Couradeau (estelle.couradeau@asu.edu)

Received: 18 December 2012 – Published in Biogeosciences Discuss.: 22 February 2013
Revised: 24 June 2013 – Accepted: 26 June 2013 – Published: 1 August 2013

Abstract. The search for microfossils in the geological record has been a long-term challenge. Part of the problem comes from the difficulty of identifying such microfossils unambiguously, since they can be morphologically confused with abiotic biomorphs. One route to improve our ability to correctly identify microfossils involves studying fossilization processes affecting bacteria in modern settings. We studied the initial stages of fossilization of cyanobacterial cells in modern microbialites from Lake Alchichica (Mexico), a Mg-rich hyperalkaline crater lake (pH 8.9) hosting currently growing stromatolites composed of aragonite [$CaCO_3$] and hydromagnesite [$Mg_5(CO_3)4(OH)_2 \cdot 4(H_2O)$]. Most of the biomass associated with the microbialites is composed of cyanobacteria. Scanning electron microscopy analyses coupled with confocal laser scanning microscopy observations were conducted to co-localize cyanobacterial cells and associated minerals. These observations showed that cyanobacterial cells affiliated with the order Pleurocapsales become specifically encrusted within aragonite with an apparent preservation of cell morphology. Encrustation gradients from non-encrusted to totally encrusted cells spanning distances of a few hundred micrometers were observed. Cells exhibiting increased levels of encrustation along this gradient were studied down to the nm scale using a combination of focused ion beam (FIB) milling, transmission electron microscopy (TEM) and scanning transmission x-ray microscopy (STXM) at the C, O and N K-edges. Two different types of aragonite crystals were observed: one type was composed of needle-shaped nano-crystals growing outward from the cell body with a crystallographic orientation perpendicular to the cell wall, and another type was composed of larger crystals that progressively filled the cell interior. Exopolymeric substances (EPS), initially co-localized with the cells, decreased in concentration and dispersed away from the cells while crystal growth occurred. As encrustation developed, EPS progressively disappeared, but remaining EPS showed the same spectroscopic signature. In the most advanced stages of fossilization, only the textural organization of the two types of aragonite recorded the initial cell morphology and spatial distribution.

1 Introduction

The search for microbial cell fossils (microfossils) in the geological record has been a long-term challenge causing multiple debates (Schopf and Packer, 1987; Brasier et al., 2002, 2005; Schopf et al., 2002, 2010). Part of the problem comes from the difficulty to identify microfossils unambiguously, since they are small and their morphology can be confused with abiotic biomorphs (Garcia-Ruiz et al., 2002). Microbialites are organosedimentary formations resulting from the microbially mediated precipitation of carbonates (Burne and Moore, 1987) and are favored targets in the search for microfossils (Riding, 2000). Stromatolites (i.e., laminated microbialites) are considered among the oldest records of life on earth (e.g., Allwood et al., 2006; Altermann and Division, 2006; Altermann, 2004; Grotzinger and Knoll, 1999).

It has been traditionally suggested that the formation of ancient stromatolites was mediated by cyanobacterial oxygenic photosynthesis based on comparison with modern analogues (Altermann et al., 2006; Riding, 2006a; Buick, 2008). A few alternative scenarios involving purely abiotic processes (Lowe, 1994; Grotzinger and Rothman, 1996; McLoughlin et al., 2008), anoxygenic photosynthesis (Bosak et al., 2007) or sulfur metabolism (Wacey et al., 2011; Bontognali et al., 2012) have been tentatively proposed. Putative cyanobacterial microfossils have been reported in the Warrawoona stromatolitic formation ($\sim$ 3.45 Ga) (Schopf and Packer, 1987) but both their biogenicity and their cyanobacterial affiliation have been questioned (Brasier et al., 2002). Microfossils of undefined taxonomic affiliation have been proposed in stromatolites from the Tumbiana formation at 2.7 Ga (e.g., Lepot et al., 2008). Interestingly, while microfossils of calcified cyanobacteria are commonly found in the geological record since the base of the Cambrian–Precambrian stromatolites most often lack microfossils, the earliest undisputed occurrence being *Girvanella* at 700 Ma (Riding, 2006a). This lack of cyanobacterial microfossils in Precambrian rocks despite the fact that stromatolites were well developed and cyanobacteria were already present since at least 2.3 Ga has been called the "Precambrian enigma"(Riding and Voronova, 1982; Arp et al., 2001; Riding, 2012). Understanding the processes leading to microfossil formation would help to understand why cyanobacteria did not get encrusted and did not fossilize in the Precambrian era.

It is assumed that the formation of cyanobacterial microfossils results from the local impregnation of their cell wall or sheath by carbonate precipitation, which is induced by photosynthetic activity (Riding, 1982, 2006a). Cyanobacteria import carbon in the form of HCO_3^- in environments where dissolved CO_2 is limiting. HCO_3^- is then converted to CO_2 and CO_3^{2-} or, depending on the authors, CO_2 and OH^- (Jansson and Northen, 2010). CO_2 is then fixed by photosynthesis into organic carbon while CO_3^{2-} and/or OH^- are exported to the extracellular medium. This raises the saturation of the surrounding solution with various carbonate minerals, depending on the cation content of the extracellular solution (e.g., Mg^{2+} and/or Ca^{2+}). An additional source of oversaturation is provided by an active export of Ca^{2+} from the cells coupled with import of H^+ (Belkin et al., 1987). Finally, cyanobacteria produce extracellular polymeric substances (EPS) that form a diffusion-limited micro-environment where pH and other chemical gradients (e.g., $[Ca^{2+}]$) build up (Arp et al., 2001). As a result, $CaCO_3$ crystals may precipitate around the cells and entomb them (e.g., Riding, 2006a; Pentecost and Franke, 2010). Alternatively, it has been suggested that the production of large amounts of EPS by cyanobacteria may inhibit carbonate precipitation by sequestering cations. In that case, prior degradation of EPS by heterotrophic bacteria may be necessary for carbonate precipitation to occur (Dupraz and Visscher, 2005).

Two types of causes, highly debated, have thus been proposed to explain the lack of Ca- and/or Mg-carbonate impregnation of cyanobacterial cells during the Precambrian. First, the chemical composition of the Precambrian ocean may have not provided suitable conditions for calcium carbonate precipitation in cyanobacterial sheaths (Arp et al., 2001). A high concentration of carbonate ions (due to a high partial pressure of carbon dioxide at that time) and a low concentration of calcium ions would promote calcium carbonate precipitation far from cells which consequently would not get encrusted, and would be thus not preserved as microfossils. Other authors argue that biological parameters such as sheath EPS composition (Dupraz and Visscher, 2005; Obst et al., 2009) and/or cell activity (Kupriyanova et al., 2011) being additional critical parameters, ancestral cyanobacteria may have not been able to provoke extracellular carbonate nucleation and precipitation efficiently (Jansson and Northen, 2010; Couradeau et al., 2012).

The mechanism of cyanobacterial calcification by sheath impregnation is still debated in several occurrences including the oldest calcified microfossils. For instance, the mechanisms leading to the formation of the *Girvanella*-type microfossils, which are widespread in Paleozoic formations, have been questioned. Based on petrographic evidence, some authors have proposed that the calcification took place *post-mortem* (Pratt, 2001); others suggest it is a result of cell metabolic activity (Arp et al., 2002). In any case, all authors agree on the fact that a better understanding of processes involved in cyanobacterial calcification in modern settings is required.

While there is an extensive record of fossil calcified cyanobacteria (Arp et al. (2001) mention 864 occurrences of fossil calcified cyanobacteria reported in the literature), only a few modern field occurrences have been studied thoroughly (Table S1).

Modern stromatolites/microbialites form in marine as well as lacustrine environments. Marine stromatolites such as Bahamas and Shark Bay stromatolites have been studied in details (e.g., Goh et al., 2009; Planavsky and Ginsburg, 2009; Reid et al., 2000; Visscher et al., 1998) and have been considered as good analogues to ancient stromatolites since they exhibit the same laminated macrofabric (see for instance R Pamela Reid et al., 2003). However, some Archean stromatolites have been shown to form in lakes e.g., those from the Tumbiana formation (2.7 Ga) (Awramik and Buchheim, 2009). Therefore, the study of lacustrine microbialites is also relevant and is needed to complete the available reference database used to interpret ancient microbialites.

In that framework, Lake Alchichica is a hyperalkaline lake (pH $\sim$ 8.9) in Mexico and harbors a high density of modern microbialites composed mostly of hydromagnesite and aragonite (Kaźmierczak et al., 2011). Recently, the systematic association of colonies of Pleurocapsales with patches of

aragonite has been evidenced in these microbialites (Gerard et al., in press). Pleurocapsales are an abundant cyanobacterial groups identified in Alchichica microbialites, which otherwise harbor a wide microbial diversity (Couradeau et al., 2011). Aragonite is usually in smaller abundance than hydromagnesite in these microbialites. Hence the precipitation of aragonite in Lake Alchichica is not the dominant process involved in the accretion of the microbialites. However, it is a particularly interesting process since it allows a delicate preservation of cells remnants and a model for the first stages of fossilization. Aragonite has been suggested as the primary phase in the Tumbiana stromatolites (e.g., Lepot et al., 2008), stressing the importance of studying modern calcification by this phase. Here, we aimed at studying at the submicrometer scale this association between Pleurocapsales and aragonite, as a modern case of cyanobacterial calcification. This allowed for getting details on the different steps of the calcification process of Pleurocapsales cells. For that purpose, we characterized the assemblages of Pleurocapsales cells and aragonite using a combination of confocal laser scanning microscopy (CLSM), scanning and transmission electron microscopies (SEM, TEM), focused ion beam (FIB) milling and synchrotron-based scanning transmission x-ray microscopy (STXM). The study of mineral growth around and within cells and resulting mineral textures as well as the assessment of the distribution of organic matter in these systems provide an unprecedented and important modern reference at the nm scale for future studies of fossil calcified cells.

2 Material and methods

2.1 Sample collection and preparation

The microbialite sample analyzed in this study was collected at a depth of 4 m in Lake Alchichica in 2007 (Kaźmierczak et al., 2011) and placed in a sterile zip plastic bag. A microbialite fragment was subsequently fixed in the laboratory in a 4 % formaldehyde solution (methanol free, ultra pure; Polysciences, Inc.) 4 h at 4 °C then washed in phosphate-buffered saline (PBS) solution and finally stored in (1/1) ethanol/PBS at −20 °C. A millimeter-sized fixed fragment was stained first by calcein at a concentration of 0.1 mg mL^{-1} for 48 h at 4 °C, then by DAPI at 1 µg mL^{-1} for 2 h at room temperature. Samples were then dehydrated through a graded series of ethanol solutions (i.e., ethanol/water volume ratios at 30 %, 50 %, 70 %, 90 %, and 100 %), and progressively embedded in hard grade LR-white resin (Polysciences, Inc.). This was followed by incubation at 4 °C for 18 h in (1/1) then (2/1) mixture of LR-white/ethanol and finally in pure LR-white resin. After 3 h at room temperature, samples were embedded in pure LR-white resin for 1 h at 40 °C and then for 24 h at 60 °C. Transverse cross sections were cut using a diamond wire before polishing using diamond powder at 1/4 µm.

2.2 Bulk x-ray diffraction (XRD)

A non-treated fragment of microbialite was ground in 100 % ethanol. XRD patterns were recorded with a Panalytical X'Pert Pro MPDH mounted in the Bragg Brentano configuration. Data were recorded with a monochromatic CoKα beam ($\lambda = 0.17889$ nm) in continuous scan mode within a (3–100°) 2θ range with steps of 0.017° and a counting time of 813.98 s per step.

2.3 Confocal laser scanning microscopy (CLSM)

Polished sections were observed using an Olympus FluoViewTM FV1000 confocal laser scanning microscope. The microscope was equipped with a 405 nm laser diode, and multi-line argon (458 nm, 488 nm, and 515 nm), helium-neon-green (543 nm) and helium-neon-red (633 nm) lasers. Fluorescence images were obtained by concomitant excitation at wavelengths of 405 nm, 488 nm, and 543 nm and collection of the emitted fluorescence between 425–475 nm, 500–530 nm, and 560–660 nm. Despite the possible occurrence of crosstalks between DAPI and autofluorescence when using simultaneous excitation, Gerard et al. (2013) have shown the efficiency of this approach on Lake Alchichica microbialites to image diverse cyanobacteria, including Pleurocapsales.

2.4 Scanning electron microscopy and FIB milling

The section of the microbialite sample collected at a 4 m depth and analyzed by CLSM was coated with gold-palladium and observed by scanning electron microscopy (SEM). Images were collected in backscattered and secondary electron modes using a Zeiss Ultra 55 FEG-SEM operating at 10 kV with a 30 µm aperture and a working distance of 8 mm. Elemental compositions were determined by energy dispersive x-ray spectrometry (EDXS) using an EDS QUANTAX detector and the software ESPRIT. EDXS analyses were operated using a 20 keV acceleration voltage, a 60 µm aperture and a working distance of 7.5 mm. Two ultrathin foils transparent to electrons (< 200 nm) were prepared by FIB milling with a Zeiss dual FIB-NEON 40EsB using the FIB "lift-out" technique (e.g., Benzerara et al., 2005). A 30 kV Ga^+ beam operated at ∼ 5 nA was used for the initial steps of the milling. Progressive excavation from both sides of the section area was performed through repeated milling of steps. Depth of milling was approximately 6 microns. An in situ micromanipulator was attached to the foil by FIB-assisted platinum deposition and the foil was liberated from the substrate by a U-cut milling pattern. The foil was transferred to an Omniprobe grid and welded to it. Final thinning of the section was performed with Ga^+ beam operated at 100 pA current. The foil measured 15 µm in length, ∼ 6 µm in width and ∼ 100–200 nm in thickness.

2.5 Transmission electron microscopy (TEM)

TEM observations were carried out on a JEOL2100F microscope operated at 200 kV, equipped with a field emission gun, a high resolution UHR pole piece, and a US4000 GATAN camera. Selected area electron diffraction (SAED) was performed using the smallest aperture allowing retrieval of diffraction patterns from a $100 \times 100\,nm^2$ area.

2.6 Scanning transmission x-ray microscopy (STXM)

Scanning transmission x-ray microscopy (STXM) and near-edge x-ray absorption fine structure (NEXAFS) spectroscopy measurements were carried out on molecular environmental science 11.0.2.2 beamline at the Advanced Light Source (ALS, Berkeley, USA).

The rationale for STXM data acquisition and analysis and examples of applications can be found in Bluhm et al. (2006) and Moffet et al. (2010). For STXM imaging, the x-ray beam is focused on an x-ray transparent sample using a zone plate, and a 2-D image is collected by scanning the sample at a fixed photon energy. The achieved spatial resolution is dependent on the zone plate (~ 25 nm in the present study) and the scanning step (which varies from one image to another). The image contrast results from differential absorption of x-rays, which partly depends on the chemical composition of the sample. In addition to imaging, it is possible to perform at the same spatial resolution, near-edge x-ray absorption fine structure (NEXAFS) spectroscopy at the carbon K-edge (and other absorption edges in the 80–2000 eV energy range) which gives information on the speciation (i.e., type of functional group and bonding) of carbon (and other elements).

Measurements were performed at the C, O and N K-edges and at the Ca $L_{2,3}$-edges. ALS storage ring was operated at 1.9 GeV and 500 mA current. Energy calibration was done using the well-resolved 3p Rydberg peak at 294.96 eV of gaseous CO_2 and the L_3 most intense peak of calcite at 349.3 eV (Benzerara et al., 2004). Methods used for STXM data acquisition and analysis and examples of STXM applications can be found, for example, in Benzerara et al. (2010, 2011) and Obst et al. (2009). AXis2000 software was used to extract NEXAFS spectra from image stack measurements and STXM map construction.

2.7 Saturation index calculation

The saturation indices of the Lake Alchichica solution with respect to aragonite and hydromagnesite were calculated for different pH (between 8 and 12) using the software Visual Minteq 3.0 and the Minteq thermodynamic database. Concentrations of major ion concentrations, total alkalinity and temperature were measured during collection of the samples and were reported in Kaźmierczak et al., 2011 (i.e., in meq L^{-1} : Cl^- 87.3 / SO_4^{2-} 16.73 / Br^- 0.1 / F^- 0.008 / Na^+ 100.5 / Mg^{2+} 35.61 / K^+ 5.32 / Ca^{2+} 0.735 / Li^+ 0.26 and alkalinity 30.9. Calculations were performed considering a temperature of 15 °C).

3 Results

3.1 SEM and CLSM analyses of cyanobacteria-mineral assemblages

Bulk XRD analyses (Fig. S1) showed that Alchichica microbialites collected at 4 m were composed of two main phases: aragonite ($CaCO_3$) and hydromagnesite ($Mg_5(CO_3)_4(OH)_2 \cdot 4H_2O$). These two mineral phases could be clearly discriminated by SEM in the backscattered electron mode (BSE): hydromagnesite appeared as light grey areas and composed the major part of the samples (85 % of the section observed), while aragonite appeared as bright discontinuous patches located preferentially at the surface of the samples in contact with microbial biofilms. The biofilms appeared as dark grey discontinuous layers lying at the surface of the microbialite and measuring 10 to 500 µm in thickness (Fig. 1a). Previous CLSM and Raman spectroscopy observations showed colonies of Pleurocapsales in contact with aragonite patches based on their typical autofluorescence and pseudo-filamentous morphology (Gerard et al., 2013). Moreover, the presence of Pleurocapsales has been consistently shown by molecular analyses based on 16S rRNA gene sequencing performed on the same sample (Couradeau et al., 2011). Here, we confirm the specific association of Pleurocapsales cells encrusted in aragonite by SEM and CLSM (Fig. 1b and c). Increasing levels of encrustation could be followed over a distance of 100 µm starting with non-encrusted cells in the biofilm at the surface of the microbialites and ending in areas where cells were completely encrusted (Fig. 2a). Calcification consisted on the formation of a mineral layer around the walls of cells that were located at the periphery of the sample. Twenty micrometers deeper in the sample, the inner part of cells was partly encrusted, still keeping a significant portion of their organic content (Fig. 2b). At fifty micrometers deep in the sample, the inner part of the cells was completely calcified and, in some cases, the cell wall was not visible anymore. Completely encrusted cells still showed some residual fluorescence by CLSM (Fig. 1c). As shown by Gerard et al. (2013) based on the acquisition of spectra, this fluorescence is specific of cyanobacterial cells and cannot be confused with the blue signal of aragonite. At this most advanced fossilization stage, encrusted cells formed some sort of pavement in the aragonite (Fig. 2a).

In order to get further insight in the mineral-cell assemblages down to the nm scale, two FIB foils were cut across encrusted cells (see locations on Figs. 2a and S2): FIB foil A was cut across partially encrusted cells located close to the surface of the microbialite; FIB foil B was cut across completely encrusted cells, which were located 44 µm deeper within the aragonite patch.

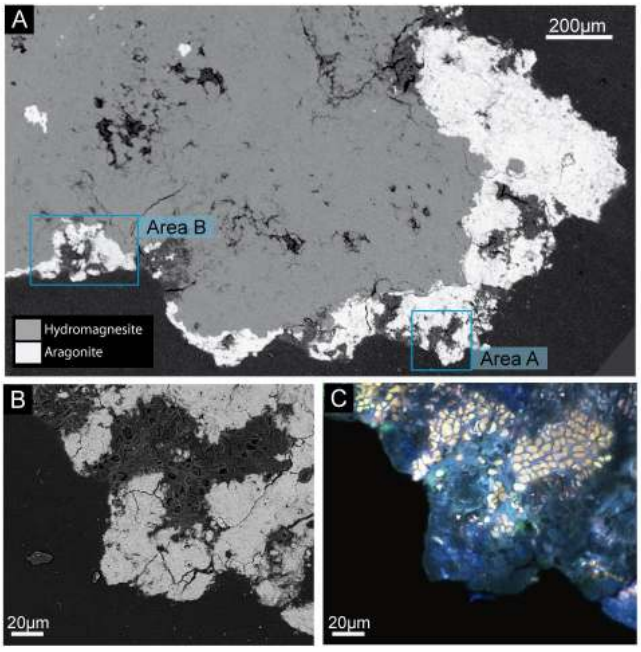

Fig. 1. Images of a section prepared from an Alchichica microbialite collected at a 4 m depth. **(A)** SEM (backscattered electron mode) picture of the section showing the relative distribution of mineral phases. Aragonite (white) lies mostly at the surface of the microbialite while hydromagnesite (light grey) composes the inner part. LR-white resin appears in dark-grey around the sample. Pockets of microorganisms are visible in aragonite, for instance in area A and area B. **(B–C)** Close-ups of area A obtained by SEM **(B)** and CLSM **(C)**. Some residual autofluorescence underline cell ghosts in the aragonitic part.

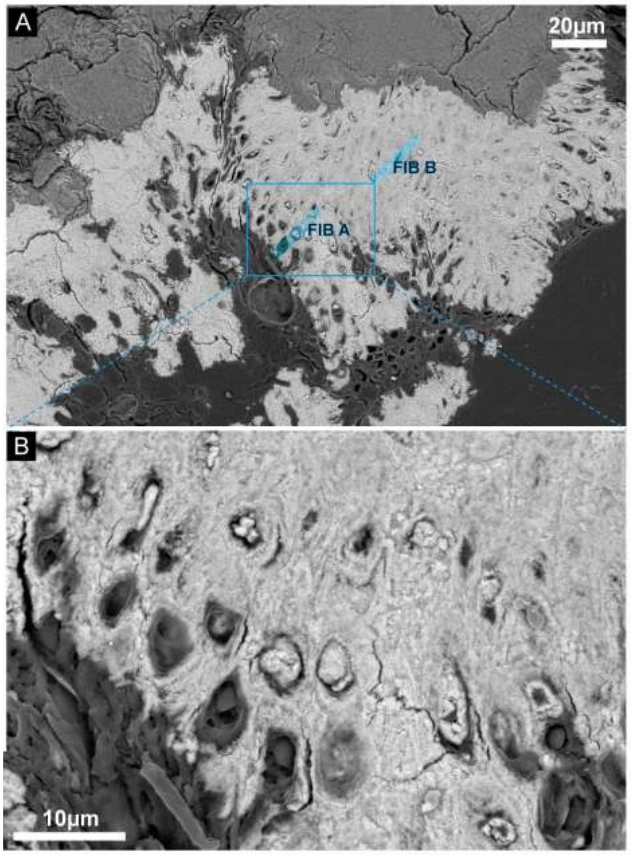

Fig. 2. Fossilization gradient of Pleurocapsales in aragonite observed by SEM in backscattered electron mode. **(A)** area B (as outlined in Fig. 1) showing progressive encrustation of cells in aragonite. Locations of FIB foils are shown. FIB foil A corresponds to the beginning of the fossilization gradient while FIB foil B was cut in totally encrusted cells. **(B)** Close-up of area B showing the textural relation between cells and aragonite. In some cells, the inner part remains totally organic while in others only the wall is visible, while the inner part being filled by aragonite.

3.2 STXM study of organic matter in the FIB foils

The distribution of carbon and calcium within FIB foils was assessed by EDX spectroscopy (Fig. S3) and the speciation of carbon (carbonates vs. organic carbon) was studied by scanning transmission x-ray microscopy (STXM). NEXAFS spectra were measured at the C K-edge on both FIB foils A and B (Fig. 3). For each foil, two types of NEXAFS spectra were observed. One type of NEXAFS spectrum was typical of calcium carbonates and showed a major peak at 290.2 eV that was attributed to 1s-$\pi*$ electronic transitions in carbonate groups (Benzerara et al., 2006). The other type of NEXAFS spectrum was characteristic of organic carbon and showed peaks at 284.8, 286.5 and 288.5 eV that could be attributed to aromatic, ketone and carboxylic functional groups, respectively (Benzerara et al., 2004). Organic carbon had the same spectroscopic signature in both FIB foils. Carbonate groups (i.e., aragonite as determined by XRD and TEM) vs. organic carbon were mapped in the two FIB foils based on their spectroscopic differences. In FIB foil A, two different textures were observed for organic carbon (Fig. 4): (i) some organic carbon appeared as homogeneous 3 micrometer wide patches filling the partly encrusted cells; (ii) the rest of the organic carbon was diffuse and showed an intimate association with aragonite crystals. Local concentrations of this organic carbon drew contour line delimiting aragonite clusters, which likely corresponded to the previous boundaries of encrusted cells (Fig. 3b). Three encrusted cells were observed in foil A (Fig. 3b). FIB foil B was cut across several cells in a more advanced encrustation stage (Figs. 2a and S2). However, only one cell could be distinguished in foil B based on a local concentration of organic carbon (Fig. 3c). Otherwise, most of the organic carbon was diffuse and intimately associated with carbonates. NEXAFS spectra were measured at the O and N K-edges (Fig. S4). Similarly to the observations performed at the C K-edge, only one kind of spectrum was retrieved from organic matter in both FIB foils, indicating that the functional groups composing organic matter as detected by NEXAFS

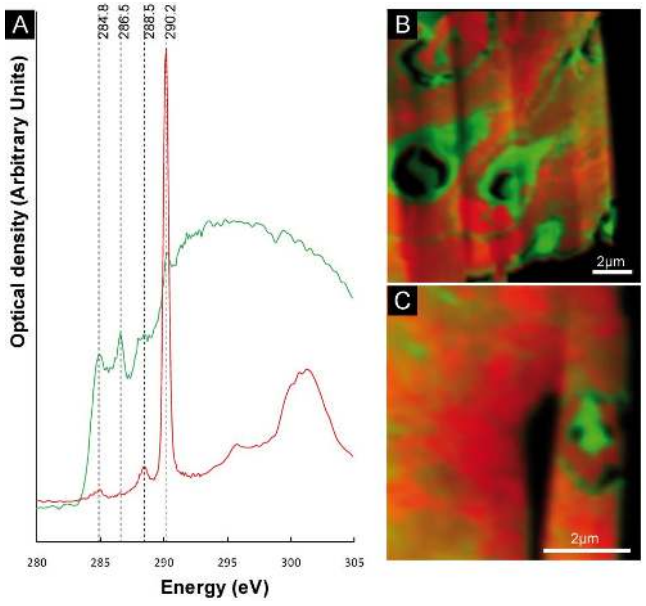

Fig. 3. Scanning transmission x-ray microscopy analyses at the C-Kedge of FIB foils A and B **(A)** NEXAFS spectra at the C K-edge of organic matter composing the cells (green) and carbonates (red). **(B)** STXM map with 40 nm spatial resolution showing the distribution of organic matter (green) and carbonate (red) in FIB foil A. Cell morphology is preserved in the first steps of fossilization. **(C)** STXM map with 40 nm spatial resolution showing the distribution of organic matter (green) and carbonate (red) in FIB foil B. The remnant of one cell can still be seen, whereas in its surroundings, the organic matter is diffuse within aragonite.

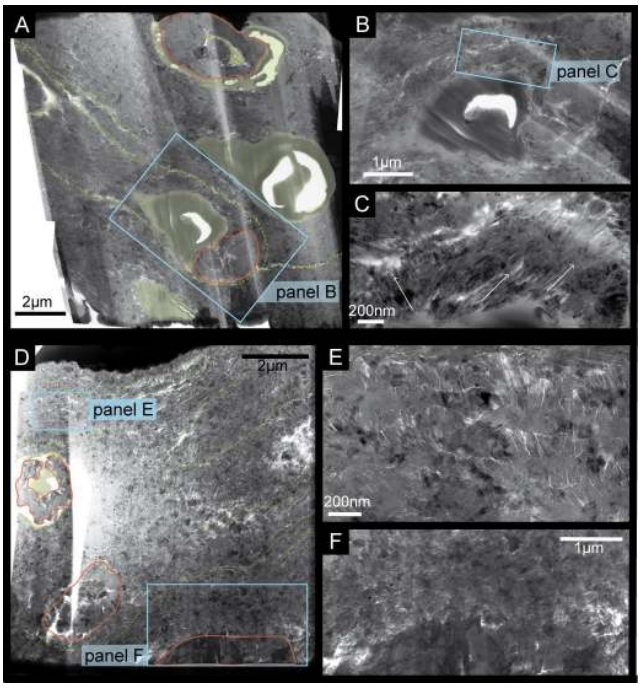

Fig. 4. TEM pictures of FIB foils A and B. **(A, D)** Picture of the whole FIB foils A and B, respectively. Organic matter appears smooth (green) while other areas are filled with fibrous aragonite (aragonite type 1) except for areas surrounded by orange lines where crystals of aragonite are bigger (aragonite type 2). Lines of less resistance in the type 1 aragonite pattern are highlighted by green dotted lines. They delineate the limits between cells. **(B)** Close-up of the area outlined in **(A)** showing an encrusted cell. **(C)** Close-up of the area outlined in **(B)** showing the radial distribution of aragonite needles at the surface of the cell. **(E)** Close-up of the area outlined in **(D)** showing the textural organization of successive aragonite type 1 layers. **(F)** Close-up of the area outlined in **(D)** showing the limit between type 1 aragonite and type 2 aragonite; no organic matter remains associated with the inner part of the cell at this stage of encrustation.

spectroscopy did not change qualitatively with increasing encrustation (Fig. S4).

3.3 Textural arrangement of aragonite crystals

Two kinds of aragonite crystals that we term in the following "type 1" and "type 2" aragonite were observed (Fig. 4). Type 1 aragonite is composed of needle-shaped nano-crystals measuring 195 ± 55 nm in length and 20 ± 5 nm in width (based on 25 measurements each on Fig. S5, see also Fig. S6). They formed clusters in which aragonite crystals shared a similar crystallographic orientation, as confirmed by selected area electronic diffraction showing arcs of restricted angular stretch (Fig. S6). Type 2 aragonite was composed of larger prismatic crystals less homogenous in size (width between 100–500 nm, see Fig. S5). In the most advanced stages of encrustation, each cell was either filled with organic matter or type 2 aragonite. For all the different stages of encrustation of Pleurocapsales, type 1 aragonite needles were perpendicular to the cell surface and formed a radial crown around the cells (Fig. 4c). The addition of radial layers of type 1 aragonite around the cells likely led to the concentric growth pattern observed in Figs. 4 and S5. This pattern results from the succession of ~ 200 nm wide layers, each of those layers composed of aragonite needles sharing a common crystallographic orientation that is intermediate between those of the layers located beneath and above. This progressive change in crystallographic orientation from one layer to the next one accommodates the transition between two encrusted cells. Interestingly, a higher concentration of organic matter was observed (Fig. 3b) in these transition areas where aragonite crystals formed around two neighboring Pleurocapsales cells converge (see dotted lines in Fig. 4a and d). The relative distribution of type 1 aragonite (outside the cells) and type 2 aragonite (within the cells) correlated with the location of encrusted cells. Owing to the mineral texture, it was therefore possible to infer the presence of former cells even when encrustation was much advanced and only little organic carbon remained (Figs. 4d–f and S5).

4 Discussion

4.1 Preferential fossilization of Pleurocapsales

A previous analysis of 16S rRNA genes showed that at least 34 phylotypes of Cyanobacteria were present in Alchichica microbialites, including 5 phylotypes of Pleurocapsales (Couradeau et al., 2011). One phylotype of Pleurocapsales (Alchichica_AL52_2_1B_148 CyanoOTU35) was particularly abundant in Alchichica samples (up to 69 % of all cyanobacteria) (Couradeau et al., 2011). The closest relative of this phylotype was detected in microbialites from Lake Van (Lopez-Garcia et al., 2005) suggesting an adaptation of this particular lineage to mineralizing environments such as alkaline lakes. Permineralization of cyanobacterial cells, including members of the Pleurocapsales, by aragonite has been proposed as an important mechanism contributing to Lake Van microbialite growth (Kempe et al., 1991; Lopez-Garcia et al., 2005). Moreover, close associations between Pleurocapsales and aragonite have been reported by other studies, e.g., in the Bahamian thrombolitic black mats (Mobberley et al., 2011) or in Satonda microbialites where the *Pleurocapsa-Dermocarpella* zone was associated with aragonite aggregates (Arp et al., 2003). In Laguna Mormona stromatolites, the permineralization of *Entophysalis*-like Pleurocapsales by aragonite was proposed as the most important mechanism of stromatolite accretion (Horodyski and Vonder Haar, 1975). Our observations further suggest that Pleurocapsales are essential players in aragonite formation and specifically contribute to the formation of Alchichica microbialites.

The Pleurocapsales are often closely associated with carbonate minerals (Table S1), suggesting that this group is especially prone to being encrusted. Assessing this ability to get encrusted among the microbial diversity associated with microbialites will be crucial to better determine the fraction of the microbial diversity that can be expected to be fossilized.

4.2 Biomineralization pattern of Pleurocapsales and fate of organic matter

In Alchichica microbialites, crystals of type 1 aragonite first appear within clusters of Pleurocapsales cells which exhibit autofluorescence and show texturally preserved traces of the cell walls at least at the SEM scale. This argues in favor of in vivo calcification. Chemical processes inducing cyanobacterial cell encrustation by calcium carbonates have been proposed by previous studies (Dupraz et al., 2009). It is classically proposed that oxygenic photosynthesis locally increases the pH in the cell vicinity leading to carbonate oversaturation and precipitation (Riding, 2006b; Jansson and Northen, 2010). Alternatively, induction of precipitation at the surface of the cells may be due to the presence of nucleating molecules such as those composing cyanobacterial sheaths (Merz-Preiss and Riding, 1999) or *S* layer proteins (Thompson et al., 1997).

Concerning the localization of mineral nucleation, two kinds of biomineralization pathways are observed in modern cases of cyanobacterial calcification as described in the literature (Table S1): (1) calcification occurs extracellularly in the biofilm by replacing EPS or (2) directly at the cell surface (on the cell wall or within the sheath), the second case being more prone to form microfossils. Arp et al. (2001) proposed a model explaining how the prominence of one calcification pathway over the other may depend on the chemical conditions of the environment. It has been suggested by Arp et al. (2001) that at low Ca^{2+}/high dissolved inorganic carbon (DIC), carbonate nucleation may occur randomly in the biofilm and not specifically in association with cyanobacterial cells. In this particular setting, the pH increase resulting from photosynthetic activity may not produce a significant local pH gradient due to the high capacity of pH buffering of the system (Arp et al., 2001). In contrast, Shiraishi (2012) observed that photosynthesis-induced carbonate precipitation can occur even at high DIC, arguing that the pH shift due to photosynthesis is not the main driver of calcification in this case. In Lake Alchichica, where low Ca^{2+}/high DIC conditions prevail, type 1 aragonite needles are organized perpendicularly to the cell wall, arguing in favor of nucleation occurring at the cyanobacterial cell surface supporting the view by Shiraishi (2012). This ability might be related to special physiological features of cyanobacteria belonging to the Pleurocapasales order and/or a particular chemical composition of the surface of the cells. For example, it has been proposed that the organization of the sheath provides a template for mineral nucleation and promotes mineral nucleation (Reitner, 1993; Braissant et al., 2003; Dupraz and Visscher, 2005). It is possible that the particular sheath of Pleurocapsales, also referred to as the fibrous layer (Waterbury and Stanier, 1978; Pinevich et al., 2008), might provide a suitable template for mineral nucleation; moreover, it is known that this kind of sheath, unlike the more common tubular sheath, is intimately attached to the cell outer membrane (Waterbury and Stanier, 1978). This particular feature might favor the formation of microfossils, since the encrusted sheath may remain connected to the cell body.

This mechanism may explain the first stage of sheath impregnation by "type 1" aragonite and its associated layered texture. The later growth of type 2 aragonite may occur post-mortem since type 2 aragonite sometimes entirely fills the cell cytoplasm. In some cyanobacterial species, calcification can occur in vivo intracellularly (Couradeau et al., 2012) but in that case, precipitates are spherical, amorphous and keep a small size below 200 nm. Post-mortem calcification processes have been suggested by other authors. For example, in modern microbialites from the Tikehau atoll, carbonate precipitation may start in vivo before pervasive precipitation due to organic matter decay (Sprachta et al., 2001). In vivo calcification allows for the preservation of the size

and the morphology of the cells (Merz-Preiss and Riding, 1999) while post-mortem calcification (Bartley, 1996) forms crystals with a morphology controlled by the geometry of the available space (Chafetz and Buczynski, 1992; Riding, 2006b). Formation of type 2 aragonite within cells may prevent a subsequent collapse of the cell overall structure during further compaction as suggested previously (Golubic and Hofmann, 1976).

Whatever the mechanism of encrustation, the most advanced stages show some traces of the cells under two forms: (1) some residual pigments are preserved as indicated by the detection of autofluorescence by CLSM. Pigments are especially recalcitrant molecules that can be preserved in sediments (Leavitt et al., 1997) and can be used as molecular fossil diagnostic for photosynthetic organisms (Brocks and Pearson, 2005); and (2) the approximate shape of the cells is preserved by the specific textural arrangement of the two types of aragonite crystals. The short-term preservation of the aragonite crystals is controlled by a delicate balance between dissolution induced by metabolisms such as fermentation and aerobic respiration and precipitation induced by metabolisms such as oxygenic or anoxygenic photosynthesis or sulfate reduction (Dupraz et al., 2009; Stal, 2012). The stability upon aging of this kind of textural biosignature remains to be assessed. It has been shown previously that very fine ultrastructural features such as cell nucleus in eukaryotes (Huldtgren et al., 2011) or cell periplasm in bacteria (Cosmidis et al., 2013; Miot et al., 2011) can occasionally be preserved by fossilization, even when rocks have been affected by metamorphism (Bernard et al., 2007; Galvez et al., 2012).

4.3 Aragonite vs. hydromagnesite precipitation

We have stressed on the point that Pleurocapsales induce carbonate precipitation at their surface possibly due to their photosynthetic activity and/or the activity of other microbes (e.g., sufate-reducing bacteria) and/or the presence of particular templating polymers at their surface. However, an additional issue is raised by our observations: why do Pleurocapsales appear specifically associated with aragonite while the bulk of Alchichica microbialites is formed by hydromagnesite? Previous studies have shown that subtle variations in the chemical composition of the solution can impact significantly the nature of precipitated mineral phases and that this can be predicted by chemical equilibrium modeling (Gallagher et al., 2013). As discussed above, several parameters are key in the induction of carbonate precipitation, including the pH. Here, we are more specifically interested in the parameters that orient the precipitation towards aragonite instead of hydromagnesite. This orientation may be driven by several factors including the concentration ratio of $[Ca^{2+}]/[Mg^{2+}]$ and pH.

A local increase in the $[Ca^{2+}]/[Mg^{2+}]$ ratio around Pleurocapsales cells could be one way of explaining why aragonite precipitation is favored over hydromagnesite. It is known that cyanobacteria contain Ca^{2+}-ATPases responsible for the transport of Ca^{2+} outside the cytoplasm (McConnaughey and Whelan, 1997). Their activity allows the maintenance of a low cytoplasmic Ca^{2+} concentration (Dominguez, 2004). This could result in the increase of the $[Ca^{2+}]/[Mg^{2+}]$ in the cyanobacterial cell vicinity. It could thus be speculated that Pleurocapsales pump out Ca^{2+} at a much higher rate than other cyanobacteria in the microbialites, which do not calcify or do not induce aragonite precipitation.

Alternatively, the control of local pH might be a key parameter in carbonate precipitation around cyanobacterial cells. The calculation of aragonite and hydromagnesite saturation index (Fig. S7) shows that both phases are oversaturated at the pH of the lake, with slightly higher saturation index for aragonite than hydromagnesite. Our calculations show that if pH increases, e.g., due to photosynthetic activity, then the saturation index of hydromagnesite would increase more than that of aragonite suggesting that higher pH would favor hydromagnesite over aragonite precipitation. This is not what is observed for Pleurocapsales in Lake Alchichica. Consequently, an increase of the $[Ca^{2+}]/[Mg^{2+}]$ ratio seems the best explanation for the orientation of the precipitation reaction towards aragonite instead of hydromagnesite. Calcium ions are usually chelated efficiently by the cyanobacterial sheaths (Braissant et al., 2009; Dupraz et al., 2009) and then released from EPS by the activity of heterotrophic bacteria, increasing their concentration and enhancing calcium carbonate precipitation (Dupraz and Visscher, 2005). Such a mechanism may apply as well to the precipitation of aragonite by Alchichica Pleurocapsales. However, the specificity of this mechanism on calcium over magnesium has never been tested experimentally, and will require further investigation with appropriate cyanobacterial strains. In the present study, we do not have data supporting or invalidating the biogenic origin of hydromagnesite. Other studies have previously discussed this point specifically (Gerard et al., 2013).

4.4 Stepwise model of fossilization in Pleurocapsales

As a summary, the fossilization pattern of Pleurocapsales within aragonite appears to proceed in four main steps (Fig. 5). In the first step, the cell is photosynthetically active and modifies the local chemical environment including the Ca^{2+}/Mg^{2+} ratio (step 1). Nucleation starts close on the cell wall, and needles of type 1 aragonite initially grow perpendicularly to cell surface, radiating towards the exterior (step 2). The morphology and growth pattern of type 1 aragonite might be controlled by surrounding organic matter (Braissant et al., 2003). Clusters of type 1 aragonite fill the space surrounding the cell and their orientation accommodates the transition from one encrusted cell to another (step 3). At this step organic matter is still detectable in the inner part of the cell. The organic matter around the cell that initially corresponded to EPS is then pushed towards the borders of cell clusters. In a final step (step 4) type 2

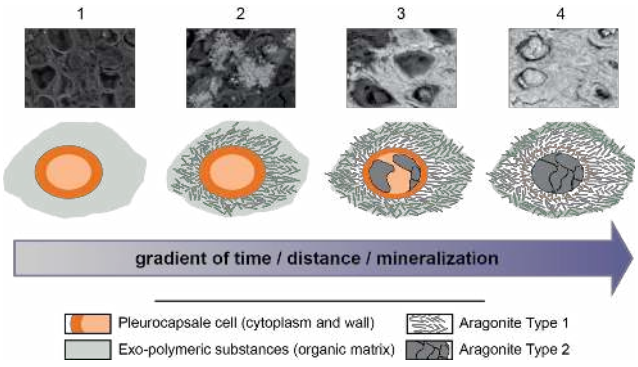

Fig. 5. Summarizing sketch of Pleurocapsales encrustation within aragonite. Each step is illustrated by a SEM picture. The mineralization gradient increases from left to right. (1) Living colony of Pleurocapsales. (2) Needles of Type 1 aragonite nucleate and grow from the surface of Pleurocapsales cells. (3) Growth of Type 1 aragonite fills the space surrounding the cell and accommodates the transition from one encrusted cell to another. The inner part is still organic and starts to be replaced by Type 2 aragonite. (4) In the end, the cell is totally filled by aragonite; an organic wall separating Type 1 from Type 2 aragonite is preserved temporarily.

aragonite precipitates within cells. Type 2 aragonite shows a prismatic texture and bigger crystals than type 1 aragonite, which exhibits the typical needle-shaped crystal. Fluorescence of some residual organic matter is detected at this step in the cell wall. However, most of the organic matter is diffuse at this stage and does not indicate the initial organization of Pleurocapsales cells anymore. In turn, the relative textural arrangement of type 1 vs. type 2 aragonite records the initial shape and distribution of cells. It has been suggested that aragonite may be replaced diagenetically by hydromagnesite in Lake Alchichica microbialites (Kazmierczak et al., 2011). Yet, the oldest microbialites on Lake Alchichica shores are mostly composed of aragonite with no hydromagnesite, supporting the idea that at least part of the aragonite and possibly calcified Pleurocapsales cells might be preserved from early diagenesis. It would be interesting to assess the stability of this kind of textural biosignature upon aging and to look for it in increasingly old fossil stromatolites.

Supplementary material related to this article is available online at: http://www.biogeosciences.net/10/5255/2013/bg-10-5255-2013-supplement.pdf.

Acknowledgements. We wish to thank especially J. Kazmierczak and B. Kramer for organizing the sampling expedition to the Alchichica Lake in 2007 and providing invaluable help during sampling to P. López-García and D. Moreira. This project was financed by the French Interdisciplinary program "Environnements planétaires et origines de la vie" (PID OPV-EPOV). The SEM/FIB facility of the Institut de Minéralogie et de Physique des Milieux Condensés is supported by Région Ile de France grant SESAME 2006 I-07-593/R, INSU-CNRS, INP-CNRS, University Pierre et Marie Curie, Paris. The JEOL JEM-2100F at IMPMC was supported by Region Ile-de-France grant SESAME 2000 E 1435, INSU-CNRS, INP-CNRS and University Pierre et Marie Curie–Paris 6. ALS-MES beamline 11.0.2 is supported by the Director, Office of Science, Office of Basic Energy Sciences, Division of Chemical Sciences, Geosciences, and Biosciences and Materials Sciences Division of the US Department of Energy at the Lawrence Berkeley National Laboratory.

Edited by: H. Kitazato

References

Allwood, A. C., Walter, M. R., Kamber, B. S., Marshall, C. P., and Burch, I. W.: Stromatolite reef from the Early Archaean era of Australia, Nature, 441, 714–718, 2006.

Altermann, W.: Precambrian Stromatolites: Problems in definition, classification, morphology and stratigraphy, in: The Precambrian Earth: Tempos and Events. Developments in Precambrian Geology, edited by: Eriksson, P. G., Altermann, W., Nelson, D. R., Mueller, W., and Catuneanu, O., Elsevier, 564–574, 2004.

Altermann, W., Kazmierczak, J., Oren, A., and Wright, T.: Cyanobacterial calcification and its rock-building potential during 3.5 billion years of Earth history, Geobiology, 4, 147–166, 2006.

Arp, G., Reimer, A., and Reitner, J.: Photosynthesis-Induced Biofilm Calcification and Calcium Concentrations in Phanerozoic Oceans, Science, 292, 1701–1704, 2001.

Arp, G., Reimer, A., Reitner, J., and Pratt, B. R.: Calcification of cyanobacterial filaments: Girvanella and the origin of lower Paleozoic lime mud: Comment and reply – Comment, Geology, 30, 579–580, 2002.

Arp, G., Reimer, A., and Reitner, J.: Microbialite formation in seawater of increased alkalinity, Satonda crater lake, Indonesia, J. Sediment. Res., 73, 105–127, 2003.

Awramik, S. M. and Buchheim, H. P.: A giant, Late Archean lake system: The Meentheena Member (Tumbiana Formation; Fortescue Group), Western Australia, Precambrian Res., 174, 215–240, 2009.

Bartley, J. K.: Actualistic taphonomy of cyanobacteria; implications for the Precambrian fossil record, Palaios, 11, 571–586, 1996.

Belkin, S., Mehlhorn, R. J., and Packer, L.: Proton Gradients in Intact Cyanobacteria, Plant Physiol., 84, 25–30, 1987.

Benzerara, K., Yoon, T. H., Tylisczak, T., Constantz, B., Spormann, A. M., and Brown, G. E.: Scanning transmission X-ray microscopy study of microbial calcification, Geobiology, 2, 249–259, 2004.

Benzerara, K., Menguy, N., Guyot, F., Vanni, C., and Gillet, P.: TEM study of a silicate-carbonate-microbe interface prepared by focused ion beam milling, Geochim. Cosmochim. Ac., 69, 1413–1422, 2005.

Benzerara, K., Menguy, N., Lopez-Garcia, P., Yoon, T. H., Kazmierczak, J., Tyliszczak, T., Guyot, F., and Brown Jr, G. E.: Nanoscale detection of organic signatures in carbonate microbialites, P. Natl. Acad. Sci. USA, 103, 9440–9445, 2006.

Benzerara, K., Meibom, A., Gautier, Q., Kazmierczak, J., Stolarski, J., Menguy, N., and Brown Jr, G. E.: Nanotextures of aragonite in stromatolites from the quasi-marine Satonda crater lake, Indonesia, Geol. Soc. Lond., Spec. Publ., 336, 211–224, 2010.

Benzerara, K., Menguy, N., Obst, M., Stolarski, J., Mazur, M., Tylisczak, T., Brown Jr, G. E., and Meibom, A.: Study of the crystallographic architecture of corals at the nanoscale by scanning transmission X-ray microscopy and transmission electron microscopy, Ultramicroscopy, 111, 1268–1275, 2011.

Bernard, S., Benzerara, K., Beyssac, O., Menguy, N., Guyot, F., Brown, G. E., and Goffe, B.: Exceptional preservation of fossil plant spores in high-pressure metamorphic rocks, Earth Planet. Sci. Lett., 262, 257–272, 2007.

Bluhm, H., Andersson, K., Araki, T., Benzerara, K., Brown Jr, G. E., Dynes, J. J., Ghosal, S., Gilles, M. K., Hansen, H. C., Hemminger, J. C., Hitchcock, A. P., Ketteler, G., Kilcoyne, A. L. D., Kneedler, E., Lawrence, J. R., Leppard, G. G., Majzlan, J., Mun, B. S., Myneni, S. C. B., Nilsson, A., Ogasawara, H., Ogletree, D. F., Pecher, K., Salmeron, M., Shuh, D. K., Tonner, B., Tyliszczak, T., Warwick, T., and Yoon, T. H.: Soft X-ray microscopy and spectroscopy at the molecular environmental science beamline at the Advanced Light Source, J. Electron Spectrosc., 150, 86–104, 2006.

Bontognali, T. R. R., Sessions, A. L., Allwood, A. C., Fischer, W. W., Grotzinger, J. P., Summons, R. E., and Eiler, J. M.: Sulfur isotopes of organic matter preserved in 3.45-billion-year-old stromatolites reveal microbial metabolism, P. Natl. Acad. Sci. USA, 109, 15146–51, 2012.

Bosak, T., Greene, S. E., and Newman, D. K.: A likely role for anoxygenic photosynthetic microbes in the formation of ancient stromatolites, Geobiology, 5, 119–126, 2007.

Braissant, O., Cailleau, G., Dupraz, C., Verrecchia, A. P., and Verrecchia, E. P.: Bacterially induced mineralization of calcium carbonate in terrestrial environments?: the role of exopolysaccharides and amino acids, J. Sediment. Res., 73, 485–490, 2003.

Braissant, O., Decho, A. W., Przekop, K. M., Gallagher, K. L., Glunk, C., Dupraz, C., and Visscher, P. T.: Characteristics and turnover of exopolymeric substances in a hypersaline microbial mat, FEMS Microbiol. Ecol., 67, 293–307, 2009.

Brasier, M. D., Green, O. R., Jephcoat, A. P., Kleppe, A. K., Van Kranendonk, M. J., Lindsay, J. F., Steele, A., and Grassineau, N. V: Questioning the evidence for Earth's oldest fossils, Nature, 416, 76–81, 2002.

Brasier, M. D., Green, O. R., Lindsay, J. F., McLoughlin, N., Steele, A., and Stoakes, C.: Critical testing of earth's oldest putative fossil assemblage from the similar to 3.5 Ga Apex Chert, Chinaman Creek, western Australia, Precambrian Res., 140, 55–102, 2005.

Brocks, J. J. and Pearson, A.: Building the biomarker tree of life, Rev. Mineral. Geochem., 59, 233–258, 2005.

Buick, R.: When did oxygenic photosynthesis evolve?, Philos. T. Roy. Soc. B, 363, 2731–2743, 2008.

Burne, R. V. and Moore, L. S.: Microbialites; organosedimentary deposits of benthic microbial communities, Palaios, 2, 241–254, 1987.

Chafetz, H. S. and Buczynski, C.: Bacterially induced lithification of microbial mats, Palaios, 7, 277–293, 1992.

Cosmidis, J., Benzerara, K., Gheerbrant, E., Esteve, I., Bouya, B., and Amaghzaz, M.: Nanometer-scale characterization of exceptionally preserved bacterial fossils in Paleocene phosphorites from Ouled Abdoun (Morocco), Geobiology, 11, 139–153, 2013.

Couradeau, E., Benzerara, K., Moreira, D., Gerard, E., Kazmierczak, J., Tavera, R., and Lopez-Garcia, P.: Prokaryotic and Eukaryotic Community Structure in Field and Cultured Microbialites from the Alkaline Lake Alchichica (Mexico), PLoS One, 6, e28767, doi:10.1371/journal.pone.0028767, 2011.

Couradeau, E., Benzerara, K., Gérard, E., Moreira, D., Bernard, S., Brown, G. E., and López-García, P.: An early-branching microbialite cyanobacterium forms intracellular carbonates, Science, 336, 459–62, 2012.

Dominguez, D. C.: Calcium signalling in bacteria, Mol. Microbiol., 54, 291–297, 2004.

Dupraz, C. and Visscher, P. T.: Microbial lithification in marine stromatolites and hypersaline mats, Trends Microbiol., 13, 429–438, 2005.

Dupraz, C., Reid, R. P., Braissant, O., Decho, A. W., Norman, R. S., and Visscher, P. T.: Processes of carbonate precipitation in modern microbial mats, Earth-Sci. Rev., 96, 141–162, 2009.

Gallagher, K. L., Braissant, O., Kading, T. J., Dupraz, C., and Visscher, P. T.: Phosphate-Related Artifacts In Carbonate Mineralization Experiments, J. Sediment. Res., 83, 37–49, 2013.

Galvez, M. E., Beyssac, O., Benzerara, K., Bernard, S., Menguy, N., Cox, S. C., Martinez, I., Johnston, M. R., and Brown Jr, G. E.: Morphological preservation of carbonaceous plant fossils in blueschist metamorphic rocks from New Zealand, Geobiology, 10, 118–129, 2012.

Garcia-Ruiz, J. M., Carnerup, A., Christy, A. G., Welham, N. J., and Hyde, S. T.: Morphology: an ambiguous indicator of biogenicity, Astrobiology, 2, 353–369, 2002.

Gerard, E., Menez, B., Couradeau, E., Moreira, D., Benzerara, K., and Lopez-Garcia, P.: Combined three-dimensional Raman and molecular fluorescence imaging reveal specific carbonate-microbe interactions in modern microbialites, ISME J., in press, doi:10.1038/ismej.2013.81 2013.

Goh, F., Allen, M. a, Leuko, S., Kawaguchi, T., Decho, A. W., Burns, B. P., and Neilan, B. A.: Determining the specific microbial populations and their spatial distribution within the stromatolite ecosystem of Shark Bay, ISME J., 3, 383–96, 2009.

Golubic, S. and Hofmann, H. J.: Comparison of Holocene and mid-Precambrian Entophysalidaceae (Cyanophyta) in stromatolitic algal mats: cell division and degradation, J. Paleontol., 50, 1074–1082, 1976.

Grotzinger, J. P. and Knoll, A. H.: Stromatolites in Precambrian carbonates: Evolutionary mileposts or environmental dipsticks?, Annu. Rev. Earth Pl. Sc., 27, 313–358, 1999.

Grotzinger, J. P. and Rothman, D. H.: An abiotic model for stromatolite morphogenesis, Nature, 383, 423–425, 1996.

Horodyski, R. J. and Vonder Haar, S. P.: Recent calcareous stromatolites from Laguna Mormona (Baja California), Mexico, J. Sediment. Res., 45, 894–906, 1975.

Huldtgren, T., Cunningham, J. A., Yin, C., Stampanoni, M., Marone, F., Donoghue, P. C. J., and Bengtson, S.: Fossilized Nuclei and Germination Structures Identify Ediacaran "Animal Embryos" as Encysting Protists, Science, 334, 1696–1699, 2011.

Jansson, C. and Northen, T.: Calcifying cyanobacteria-the potential of biomineralization for carbon capture and storage, Curr. Opin. Biotechnol., 21, 365–371, 2010.

Kaźmierczak, J., Kempe, S., Kremer, B., López-García, P., Moreira, D., and Tavera, R.: Hydrochemistry and microbialites of the al-

kaline crater lake Alchichica, Mexico, Facies, 57, 1–28, 2011.
Kempe, S., Kazmierczak, J., Landmann, G., Konuk, T., Reimer, A., and Lipp, A.: Largest Known Microbialites Discovered in Lake Van, Turkey, Nature, 349, 605–608, 1991.
Kupriyanova, E. V, Sinetova, M. A., Markelova, A. G., Allakhverdiev, S. I., Los, D. A., and Pronina, N. A.: Extracellular β-class carbonic anhydrase of the alkaliphilic cyanobacterium Microcoleus chthonoplastes, J. Photochem. Photobio. B, 103, 78–86, 2011.
Leavitt, P. R., Vinebrooke, R. D., Donald, D. B., Smol, J. P., and Schindler, D. W.: Past ultraviolet radiation environments in lakes derived from fossil pigments, Nature, 388, 457–459, 1997.
Lepot, K., Benzerara, K., Brown Jr, G. E., and Philippot, P.: Microbially influenced formation of 2,724-million-year-old stromatolites, Nat. Geosci., 1, 118–121, 2008.
Lopez-Garcia, P., Kazmierczak, J., Benzerara, K., Kempe, S., Guyot, F., and Moreira, D.: Bacterial diversity and carbonate precipitation in the giant microbialites from the highly alkaline Lake Van, Turkey, Extremophiles, 9, 263–274, 2005.
Lowe, D. R.: Abiological origin of described stromatolites older than 3.2 Ga, Geology, 22, 387–390, 1994.
McConnaughey, T. A. and Whelan, J. F.: Calcification generates protons for nutrient and bicarbonate uptake, Earth-Sci. Rev., 42, 95–117, 1997.
McLoughlin, N., Wilson, L. A., and Brasier, M. D.: Growth of synthetic stromatolites and wrinkle structures in the absence of microbes – implications for the early fossil record, Geobiology, 6, 95–105, 2008.
Merz-Preiss, M. and Riding, R.: Cyanobacterial tufa calcification in two freshwater streams: ambient environment, chemical thresholds and biological processes, Sediment. Geol., 126, 103–124, 1999.
Miot, J., Maclellan, K., Benzerara, K., and Boisset, N.: Preservation of protein globules and peptidoglycan in the mineralized cell wall of nitrate-reducing, iron(II)-oxidizing bacteria: a cryo-electron microscopy study, Geobiology, 9, 459–470, 2011.
Mobberley, J. M., Ortega, M. C., and Foster, J. S.: Comparative microbial diversity analyses of modern marine thrombolitic mats by barcoded pyrosequencing, Environ. Microbiol., 14, 82–100, 2011.
Moffet, R. C., Tivanski, A. V., and Gilles, M. K.: Chapter 17: Scanning Transmission X-ray Microscopy: Applications in Atmospheric Aerosol Research, in: Fundamentals and Applications in Aerosol Spectroscopy, edited by: Signorell, R. and Reid, J. P., 2010.
Obst, M., Dynes, J. J., Lawrence, J. R., Swerhone, G. D. W., Benzerara, K., Karunakaran, C., Kaznatcheev, K., Tyliszczak, T., and Hitchcock, A. P.: Precipitation of amorphous CaCO(3) (aragonite-like) by cyanobacteria: A STXM study of the influence of EPS on the nucleation process, Geochim. Cosmochim. Ac., 73, 4180–4198, 2009.
Pentecost, A. and Franke, U.: Photosynthesis and calcification of the stromatolitic freshwater cyanobacterium Rivularia, Eur. J. Phycol., 45, 345–353, 2010.
Pinevich, A. V., Averina, S. G., Gavrilova, O. V., and Migunova, A. V.: Baeocytes in the cyanobacterium Pleurocapsa sp.: Characterization of the differentiated cells produced by multiple fission, Microbiology, 77, 71–78, 2008.
Planavsky, N. and Ginsburg, R. N.: Taphonomy of Modern Marine Bahamian Microbialites, Palaios, 24, 5–17, 2009.
Pratt, B. R.: Calcification of cyanobacterial filaments: Girvanella and the origin of lower Paleozoic lime mud, Geology, 29, 763–766, 2001.
Reid, R. P., Visscher, P. T., Decho, A. W., Stolz, J. F., Bebout, B. M., Dupraz, C., Macintyre, L. G., Paerl, H. W., Pinckney, J. L., Prufert-Bebout, L., Steppe, T. F., and DesMarais, D. J.: The role of microbes in accretion, lamination and early lithification of modern marine stromatolites, Nature, 406, 989–992, 2000.
Reid, R. P., James, N. P., Macintyre, I. G., Dupraz, C. P., Burne, R. V., and Macintyre, G.: Shark Bay Stromatolites?: Microfabrics and Reinterpretation of Origins, Facies, 49, 299–324, 2003.
Reitner, J.: Modern Cryptic Microbialites/Metazoan Facies from Lizard island (Great Barrier Reef, Australia) Formation and Concepts, Facies, 29, 3–40, 1993.
Riding, R.: Cyanophyte calcification and changes in ocean chemistry, Nature, 299, 814–815, 1982.
Riding, R.: Microbial carbonates?: the geological record of calcified bacterial-algal mats and biofilms, Sedimentology, 47, 179–214, 2000.
Riding, R.: Microbial carbonate abundance compared with fluctuations in metazoan diversity over geological time, Sedimentary Geology, 185, 229–238, 2006a.
Riding, R.: Cyanobacterial calcification, carbon dioxide concentrating mechanisms, and Proterozoic–Cambrian changes in atmospheric composition, Geobiology, 4, 299–316, 2006b.
Riding, R.: A hard life for cyanobacteria, Science, 336, 427–8, 2012.
Riding, R. and Voronova, L.: Calcified cyanophytes and the precambrian-cambrian transition, Naturwissenschaften, 69, 498–499, 1982.
Schopf, J. W. and Packer, B. M.: Early Archean (3.3-Billion to 3.5-Billion-Year-Old) Microfossils from Warrawoona Group, Australia, Science, 237, 70–73, 1987.
Schopf, J. W., Kudryavtsev, A. B., Agresti, D. G., Wdowiak, T. J., and Czaja, A. D.: Laser-Raman imagery of Earth's earliest fossils, Nature, 416, 73–76, 2002.
Schopf, J. W., Kudryavtsev, A. B., Sugitani, K., and Walter, M. R.: Precambrian microbe-like pseudofossils: A promising solution to the problem, Precambrian Res., 179, 191–205, 2010.
Shiraishi, F.: Chemical conditions favoring photosynthesis-induced $CaCO_3$ precipitation and implications for microbial carbonate formation in the ancient ocean, Geochim. Cosmochim. Ac., 77, 157–174, 2012.
Sprachta, S., Camoin, G., Golubic, S., and Le Campion, T.: Microbialites in a modern lagoonal environment: nature and distribution, Tikehau atoll (French Polynesia), Palaeogeogr. Palaeocl., 175, 103–124, 2001.
Stal, L.: Cyanobacterial Mats and Stromatolites, in: Ecology of Cyanobacteria II, edited by: Whitton, B. A., 65–125, Springer Netherlands, 2012.
Thompson, J. B., Schultze-Lam, S., Beveridge, T. J., and Des Marais, D. J.: Whiting events: biogenic origin due to the photosynthetic activity of cyanobacterial picoplankton, Limnol. Oceanogr., 42, 133–141, 1997.
Visscher, P. T., Reid, R. P., Bebout, B. M., Hoeft, S. E., Macintyre, I. G., and Thompson, J. A.: Formation of lithified micritic laminae in modern marine stromatolites (Bahamas): The role of sulfur

cycling, Am. Mineral., 83, 1482–1493, 1998.

Wacey, D., Kilburn, M. R., Saunders, M., Cliff, J., and Brasier, M. D.: Microfossils of sulphur-metabolizing cells in 3.4-billion-year-old rocks of Western Australia, Nat. Geosci., 4, 698–702, 2011.

Waterbury, J. B. and Stanier, R. Y.: Patterns of Growth and Development in Pleurocapsalean Cyanobacteria, Microbiol. Mol. Biol. R., 42, 2–44, 1978.